remote sensing

MDPI

Article

Comparative Analysis on the Estimation of Diurnal Solar-Induced Chlorophyll Fluorescence Dynamics for a Subtropical Evergreen Coniferous Forest

Jinghua Chen [1], Shaoqiang Wang [1,2,3,*], Bin Chen [1,2], Yue Li [4], Muhammad Amir [1,2], Li Ma [1,2], Kai Zhu [1,2], Fengting Yang [1,2], Xiaobo Wang [1,2], Yuanyuan Liu [1,2], Pengyuan Wang [1,2], Junbang Wang [1,2], Mei Huang [1,2] and Zhaosheng Wang [1,2]

[1] Key Laboratory of Ecosystem Network Observation and Modeling, Institute of Geographic Sciences and Natural Resources Research, Chinese Academy of Sciences, Beijing 100101, China; chenjh.14b@igsnrr.ac.cn (J.C.); chenbin@igsnrr.ac.cn (B.C.); mamir2019@igsnrr.ac.cn (M.A.); mali.16b@igsnrr.ac.cn (L.M.); zhuk.20b@igsnrr.ac.cn (K.Z.); yangft@igsnrr.ac.cn (F.Y.); wangxiaobo17@mails.ucas.ac.cn (X.W.); liuyuanyuan182@mails.ucas.ac.cn (Y.L.); wangpy.19b@igsnrr.ac.cn (P.W.); jbwang@igsnrr.ac.cn (J.W.); huangm@igsnrr.ac.cn (M.H.); wangzs@igsnrr.ac.cn (Z.W.)

[2] College of Resources and Environment, University of Chinese Academy of Sciences, Beijing 100049, China

[3] School of Geography and Information Engineering, China University of Geosciences, Wuhan 430074, China

[4] School of Earth Science and Engineering, Hebei University of Engineering, Handan 056038, China; liyue@hebeu.edu.cn

* Correspondence: sqwang@igsnrr.ac.cn

Citation: Chen, J.; Wang, S.; Chen, B.; Li, Y.; Amir, M.; Ma, L.; Zhu, K.; Yang, F.; Wang, X.; Liu, Y.; et al. Comparative Analysis on the Estimation of Diurnal Solar-Induced Chlorophyll Fluorescence Dynamics for a Subtropical Evergreen Coniferous Forest. *Remote Sens.* **2021**, *13*, 3143. https://doi.org/10.3390/rs13163143

Academic Editor: Shawn C. Kefauver

Received: 27 May 2021
Accepted: 6 August 2021
Published: 9 August 2021

Abstract: Solar-induced chlorophyll fluorescence (SIF) is considered as a prospective indicator of vegetation photosynthetic activity and the ecosystem carbon cycle. The current coarse spatial-temporal resolutions of SIF data from satellite missions and ground measurements still cannot satisfy the corroboration of its correlation with photosynthesis and carbon flux. Practical approaches are needed to be explored for the supplementation of the SIF measurements. In our study, we clarified the diurnal variations of leaf and canopy chlorophyll fluorescence for a subtropical evergreen coniferous forest and evaluated the performance of the canopy chlorophyll concentration (CCC) approach and the backward approach from gross primary production (GPP) for estimating the diurnal variations of canopy SIF by comparing with the Soil Canopy Observation Photosynthesis Energy (SCOPE) model. The results showed that the canopy SIF had similar seasonal and diurnal variations with the incident photosynthetically active radiation (PAR) above the canopy, while the leaf steady-state fluorescence remained stable during the daytime. Neither the CCC nor the raw backward approach from GPP could capture the short temporal dynamics of canopy SIF. However, after improving the backward approach with a correction factor of normalized PAR incident on leaves, the variation of the estimated canopy SIF accounted for more than half of the diurnal variations in the canopy SIF (SIF_{687}: $R^2 = 0.53$, $p < 0.001$; SIF_{760}: $R^2 = 0.72$, $p < 0.001$) for the subtropical evergreen coniferous forest without water stress. Drought interfered with the utilization of the improved backward approach because of the decoupling of SIF and GPP due to stomatal closure. This new approach offers new insight into the estimation of diurnal canopy SIF and can help understand the photosynthesis of vegetation for future climate change studies.

Keywords: chlorophyll fluorescence; model comparison; SCOPE model; evergreen conifer; water stress

1. Introduction

Chlorophyll Fluorescence (ChlF) is regarded as a prospective marker of vegetation photosynthetic activity and a vital indicator of the carbon cycle. Leaf chlorophyll molecules capture light energy and transmit it to the reaction centers to release through three pathways:

photochemistry to drive photosynthesis, non-photochemical quenching (NPQ, i.e., thermal energy dissipation) and a small part re-emitted as ChlF [1,2]. The physics-physiology mechanism linking the photosynthetic function to ChlF indicates that the fluorescence can be an observable and valid indicator of vegetation photosynthetic activity. With the recent advancements in remote sensing techniques, solar-induced chlorophyll fluorescence (SIF) can be detected by remote sensing instruments and has been found to be correlated with gross photosynthetic carbon dioxide (CO_2) assimilation or gross primary production (GPP) at the canopy and landscape scales [3–6]. Numerous satellite missions provide space-borne SIF datasets, including GOSAT [7], GOME-2 [8], SCIAMACHY [9], OCO-2 [10], TROPOMI [11] and TANSAT [12]. Therefore, the application of fluorescence signals to derive plant photosynthesis for regional and global carbon cycle research has received increasing attention.

However, those satellite sensors only provide SIF data as passage grids, with a spatial resolution of at most several kilometers and unsatisfactory space coverage. Global satellite-based SIF data are only aggregated to biweekly and monthly at a coarse spatial resolution of 1° and 0.5° (e.g., OCO-2 and GOME-2). Spectroradiometer systems, which offer continuous tower-based SIF measurements at the canopy level, have gradually popularized. The systems semi-synchronously measure solar irradiance and plant canopy radiance for calculating the canopy SIF signals. Tower-based SIF observation systems include FluoSpec [6,13], AutoSIF [14], FloX [15], PhotoSpec [16], FAME [17] and SIFspec [18], offering an opportunity to bridge the measurement gap between satellites and carbon flux towers. ChinaSpec, a network of collaborating sites to conduct ground-based continuous SIF measurements along with flux for ecosystem research, has founded starting in 2016 and been used to assist in the validation of fluorescence models and satellite SIF products [19]. However, the distribution of these sites is still too limited to verify the satellite SIF data for multi-biome and large-scale studies so far. Thus, more SIF data resources are still needed for the verification of satellite observations and the corroboration of its correlation with photosynthesis.

Process models have been considered to be helpful approaches for quantifying the ecosystem processes and supplementing the limited practical measurements. SCOPE (Soil Canopy Observation Photosynthesis Energy) model [20] has been used proverbially as an essential tool for estimating continuous SIF and exploring fluorescence-photosynthesis linkages at different temporal scales. Holding a complete physiological expression of photosynthesis and fluorescence process, SCOPE has been considered to be a robust and reliable model for comprehending SIF and photosynthetic status in numerous research [21–23]. However, SCOPE model requests lots of input data, including leaf traits, leaf biochemical, canopy structure, meteorology and geometry, which might be difficult to obtain fully. SIF has usually been found sensitive to leaf chlorophyll content (Cab) and leaf area index (LAI) by a global sensitivity analysis using the SCOPE model [24]. Depending on that, an approach for estimating SIF at landscape and seasonal scale was established using the empirical non-linear logarithmic relationship between SIF and a product of Cab and LAI (i.e., canopy chlorophyll concentration, CCC) [25]. Except that, a forward GPP estimation approach based on canopy SIF measurement and leaf ChlF parameter was proven useful for the estimation of GPP dynamics [26], which implies whether we can use a backward way from measured GPP as a new alternative approach for canopy SIF estimation. An evaluation of these two approaches is needed for better interpreting the temporal dynamics of the SIF signal, especially for the diurnal dynamics.

Subtropical forests, a widely distributed ecosystem in southern China, are crucial to the regional and even global carbon cycle because of their high carbon sequestration capacity. It was estimated that the total annual net ecosystem production (NEP) of monsoon subtropical forests in East Asia accounted for 8% of the global forest NEP [27]. A recent study reported that the rapid increase of afforestation in the past 30 years resulted in the large carbon sink in mainland China, especially in Southwest China, in which the carbon uptake accounted for approximately one-third of the carbon uptake in mainland

China [28]. Due to the highly significant correlation of chlorophyll fluorescence and photosynthesis, accurately quantifying the SIF dynamics of this vital ecosystem is essential both for verifying satellite observation data and interpreting the underlying driving forces in the global terrestrial carbon cycle.

Therefore, the practical issue is how we can accurately estimate SIF for the subtropical evergreen coniferous forests. We evaluated the performances of two approaches, i.e., (1) the CCC approach and (2) the backward approach from GPP, for diurnal SIF estimation using measured and simulated data for a typical subtropical evergreen coniferous forest site in eastern China. In this study, our objectives are: (1) interpreting the diurnal dynamics of chlorophyll fluorescence (F_s and SIF) of a subtropical evergreen coniferous forest; (2) quantitatively evaluating the performance of the two approaches for estimating SIF by comparing with the timulation of the SCOPE model.

2. Materials and Methods

2.1. Study Site

The study was conducted at the flux tower of the Qianyanzhou (QYZ) Ecological Research Station (26°44′48″ N, 115°04′13″ E, elevation 110.8 m), located in the Ji'an, Jiangxi Province in southern China (Figure 1). QYZ site has a typical subtropical monsoon climate. The annual average solar radiation is 4661 MJ·m^{-2} and the annual average air temperature is 17.9 °C. The annual average precipitation is 1485.1 mm and the rainfall occurs mainly from March to June. The soil taxonomy of the site is red soil. The evergreen coniferous forest covers 90% of the flux tower surrounding area. Major species including *Pinus massoniana*, *Pinus elliottii* occupy more than 95% of the evergreen coniferous plantation plot, which was established in the 1980s [29]. The mean canopy height of the forest is 15.5 m [30].

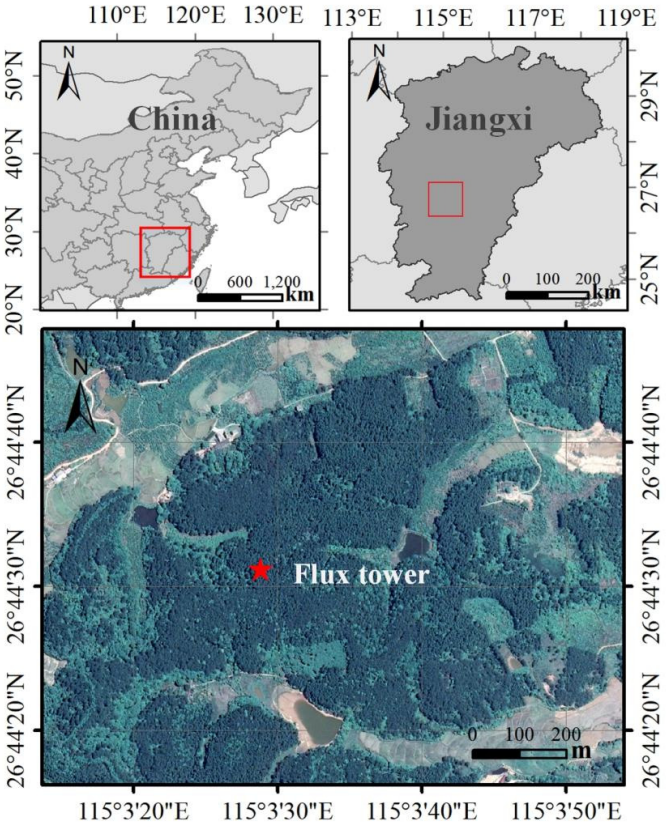

Figure 1. Location of the flux tower at Qianyanzhou (QYZ) site.

2.2. In Situ Measurements

2.2.1. Eddy Flux and Ancillary Measurement

Eddy covariance (EC) system was fixed at the height of 23 m on the flux tower to measure the net ecosystem exchange of CO_2 (NEE). The EC system comprises an open-path infrared gas analyzer (LI-7500, LI-COR Inc., Lincoln, NE, USA) for the measurement of CO_2/H_2O concentrations and a three-dimensional sonic anemometer (CSAT3, Campbell Scientific Inc., Logan, UT, USA) for the measurement of wind speed and virtual temperature. All raw EC data were recorded at 10 Hz frequency by a data logger (CR5000, Campbell Scientific, Logan, UT, USA) and then stored as the 30 min average of the EC data. Data quality control and processing were conducted using the EddyPro software (LI-COR Inc., Lincoln, NE, USA) for the production of NEE estimates. A flux partitioning algorithm [31] was employed to estimate EC-measured GPP (GPP_{EC}) using NEE and daytime ecosystem respiration (R_e).

$$GPP_{EC} = -NER + R_e \quad (1)$$

Ancillary environmental variables at canopy level were measured synchronously with EC flux measurements. The environmental variables included downward shortwave radiation (R_{in}) and longwave radiation (R_{li}) (CMP11, Kipp & Zonen, Delft, The Netherlands), PAR incident above the canopy (PAR_{canopy}) (LI-190SB, LI-COR Inc., Lincoln, NE, USA), air temperature (Ta) (HMP45C, Vaisala Group, Helsinki, Finland), air pressure (p) and atmospheric vapor pressure (ea) (CS105, Vaisala Group, Helsinki, Finland), wind speed (u) (A100R, Vector Instruments, North Wales, UK) and volumetric soil moisture content (SMC, 20 cm depth) (CS615-L, Campbell Scientific Inc., Logan, UT, USA).

2.2.2. Canopy Reflectance

The AMSPEC II spectra system [32] was installed at 31 m height of the flux tower to measure the reflectance of the canopy. The system consists of a UniSpec-DC dual-channel spectrometer (PP Systems, Amesbury, MA, USA), a PTU-D46 automatic tilt rotation device (FLIR Systems, Goleta, CA, USA), a computer and some accessories [30]. The spectrometer is equipped with both up-looking and down-looking fibers and covers a spectral range from around 300 to 1100 nm with 256 contiguous bands and 3.1–3.4 nm of FWHM. The up-looking fiber equipped with a cosine receptor is used to collect hemisphere incident irradiance, while the down-looking bare fiber simultaneously measures canopy radiance with an instantaneous field of view (IFOV) of 20°. Then, the canopy reflectance was calculated to be the ratio of the canopy radiance and incident irradiance, see [30] for details. The canopy reflectance was sampled every 2–3 s and recorded every 15 min from sunrise to sunset [33].

2.2.3. Leaf Chlorophyll Fluorescence and Photosynthesis Rates

Leaf chlorophyll fluorescence and photosynthesis rates of two major species (i.e., *Pinus massoniana* and *Pinus elliottii*) were measured on a wooden platform of 14 m height next to the flux tower. An open gas exchange system (LI-6400XT, LI-COR Inc., Lincoln, NE, USA) with an integrated leaf chamber fluorometer (LCF) (LI-6400-40, LI-COR Inc., Lincoln, NE, USA) was used to simultaneously measure the leaf chlorophyll fluorescence and photosynthesis rates. Meanwhile, some environmental variables at the leaf level were measured, including the PAR incident on the leaves (PAR_{leaf}), leaf temperature and leaf humidity. We randomly selected 3 clusters of the upper canopy needles of each species for in situ measurement every month during the 2017 growing season, namely 21 April, 22 May, 1 July, 22 July, 31 August, 24 September, 23 October and 25 November. When we used LI-6400XT to measure, the cluster of needles was flattened and they covered the entire leaf chamber to avoid measurement errors caused by overlapping leaves or gaps between leaves [33].

The selected needles were wrapped in tin foil for at least 30 min [34] before the dark-adapted measurements at around 8:00. Then, they were measured once an hour for light-adapted measurements till 17:00. After being placed in the dark for at least 30 min,

the leaves were shined on by a weak red light from the LCF and the initial minimum fluorescence (F_o) was detected. Net photosynthetic rate (P_{net}, μmol m^{-2} s^{-1}) of the leaves was recorded together with the measurements of F_o. The P_{net} under dark-adapted light ambient was regarded as dark respiration. Next, when the leaves were exposed to a saturating pulse, the fluorescence immediately rose to an initial maximal level (F_m) [26]. After the dark-adapted process, all leaves were exposed to ambient light to prepare for the light-adapted process. In this process, LCF provided an actinic light at an intensity equal to the ambient light. Then, the steady-state fluorescence (F_s) and P_{net} were recorded once they fluctuated in allowed ranges after the leaves were illuminated for 20–30 min. The P_{net} was quantified under an ambient-synchronized light intensity (i.e., PAR_{leaf}) and CO_2 level, except for the first measurement under a dark-adapted light ambient. Then, the leaf apparent photosynthesis ($P_{apparent}$) was calculated as the sum of dark respiration and P_{net} at a given ambient light intensity [35].

2.2.4. Leaf Traits and Canopy Structure

After each photosynthetic measurement, a Chlorophyll Content Meter CCM 300 (Opti-Sciences, Inc., Hudson, NH, USA) was used to measure the Cab of the same leaves (Table 1). The chlorophyll contents of leaves were measured at least five times and averaged for the final values. Plant canopy analyzer LAI-2200 (LI-COR Inc., Lincoln, NE, USA) was used to measure the effective LAI (i.e., LAI_e) on the same day as leaf fluorescence and photosynthesis measurements. In order to minimize the impact of multiple scattering of solar radiation, we measured LAI_e at overcast days or near sunset [36]. We averaged around thirty values to obtain the final LAI_e value of the day. Then, the effect of foliage clumping was considered on true LAI ($LAI = (1 - \alpha) \times LAI_e \times \gamma_E/\Omega_E$) with average shoot projected area ($\alpha = 0.07$ [37]), needle-to-shoot area ratio ($\gamma_E = 1.45$ [38]) and clumping index ($\Omega_E = 0.81$ [38]). The maximum rate of Rubisco carboxylation (V_{cmax}) was obtained from [33], which observed the same tree species during the same period.

Table 1. Leaf chlorophyll content (Cab) and canopy structure variable (LAI) used in this study.

Date	21 April	22 May	1 July	22 July	31 August	24 September	23 October	25 November
Cab (μg cm^{-2})	43.53 ± 3.51	43.83 ± 3.14	45.42 ± 3.25	41.76 ± 3.82	40.87 ± 6.36	43.48 ± 5.38	46.23 ± 5.59	42.88 ± 3.26
LAI (m^2 m^{-2})	4.31 ± 0.58	4.37 ± 1.07	4.56 ± 0.49	4.85 ± 1.07	4.63 ± 0.62	4.41 ± 0.68	4.37 ± 0.40	4.24 ± 0.48

2.3. SIF Simulation by SCOPE Model

2.3.1. SCOPE Model Description

We used the SCOPE model to retrieve vegetation parameters from the measured canopy reflectance (Ref) and then to simulate the canopy SIF (SIF_{SCOPE}). SCOPE is an integrated energy balance and radiative transfer model [20,39], which integrates the energy balance process with the radiative transfer of solar radiation (RTMo), thermal radiation emitted by the vegetation (RTMt) and re-emission as fluorescence (RTMf). In the energy balance process, a biochemical module processes the emission efficiency of fluorescence according to the other two energy de-excitation pathways: photochemical quenching via photochemical and non-photochemical quenching via heat dissipation. SCOPE can complete the calculations of canopy reflected radiation, thermal radiation and SIF in company with energy, carbon and water flux. In our study, we applied SCOPE version 2.0 to simulate SIF_{SCOPE}. To perform the simulation, the model needs input data associated with leaf optical and biochemical properties, canopy structure, meteorology and sun-view geometry (Table 2) [21]. The major input variables were derived from field measurements and model inversion. Other required variables of the SCOPE model were assumed as their default values. Our analysis concentrated on the SIF estimation results at 687 nm and 760 nm (SIF_{687} and SIF_{760}), standing for the red and far-red solar-induced fluorescence, respectively.

Table 2. Major input data of SCOPE model used in our study.

Variables	Definition	Unit	Range	Value/Source
		Leaf traits		
Cab	chlorophyll a and b content	μg cm^{-2}	0–100	measurement
Cca	carotenoid content	μg cm^{-2}	0–25	inversion
Cdm	dry matter content	g cm^{-2}	0–0.02	inversion
Cw	equivalent water thickness	cm	0–0.2	inversion
Cs	brown pigments	a.u.	0–1	inversion
N	leaf structure parameter	–	1–3.5	inversion
		Leaf biochemical		
Vcmax	maximum rate of Rubisco carboxylation (at optimum temperature)	μmol m^{-2} s^{-1}	0–200	literature
m	Ball-Berry stomatal conductance parameter	–	5–20	9
		Canopy structure		
LAI	leaf area index	m^2 m^{-2}	0–7	measurement
hc	vegetation height	m	/	measurement
LIDFa	leaf inclination	–	−1–1	inversion
LIDFb	variation in leaf inclination	–	−1–1	inversion
leafwidth	leaf width	m	/	0.001
		Meteorology		
R_{in}	broadband incoming shortwave radiation	W m^{-2}	0–1400	measurement
R_{li}	broadband incoming longwave radiation	W m^{-2}	200–500	measurement
Ta	air temperature	°C	−10–50	measurement
p	air pressure	hPa	900–1100	measurement
ea	atmospheric vapor pressure	hPa	0–60	measurement
u	wind speed at canopy height	m s^{-1}	0–50	measurement
SMC	volumetric soil moisture content	%	5–55	measurement
		Geometry		
LAT	latitude	decimal deg	/	measurement
LON	longitude	decimal deg	/	measurement
tto	observation zenith angle	decimal deg	0–60	0

2.3.2. Parameter Inversion and SIF Simulation

The values of some vegetation parameters (see details in Table 2) were retrieved from the reflectance apectra (400 to 850 nm) using the optical radiative transfer routine of SCOPE (i.e., RTMo). We used the numerical optimization (NO) method for the retrieval of required leaf and canopy parameters (Cca, Cdm, Cw, Cs, N, LIDFa and LIDFb). NO method aims to minimize the cost function that quantifies the difference between measured and simulated data by successively changing the input parameters. One set of parameter values were retrieved separately for each of the measurement days, using the canopy reflectance measured at midday [40]. Before the method started, the measured canopy reflectance spectra were linearly interpolated to a resolution of 1 nm to match the simulated one. We used the 'lsqnonlin' function listed in the optimization toolbox of MatlabR2017 and chose the 'Trust Region algorithm' for updating the values of required parameters within the ranges in [41]. With the retrieved vegetation parameters and half-hourly meteorological variables as input, we simulated diurnal cycles of SIF (SIF_{SCOPE}, i.e., SIF_{687} and SIF_{760}), GPP (GPP_{SCOPE}) and canopy reflectance (Ref_{SCOPE}) using the full SCOPE model. The SCOPE model outputs the net canopy photosynthesis, representing the total gross photosynthesis minus the CO_2 flux caused by leaf respiration [21]. Therefore, we added the total photosynthesis rate of leaf as one of the outputs for the codes of the biochemical module in the SCOPE model, then the total gross photosynthesis rate of the canopy, known as GPP_{SCOPE}, was calculated as the same way of net photosynthesis. The measured GPP_{EC} and Ref were compared with the simulated ones to validate the accuracy of SCOPE model simulation (Figure 2).

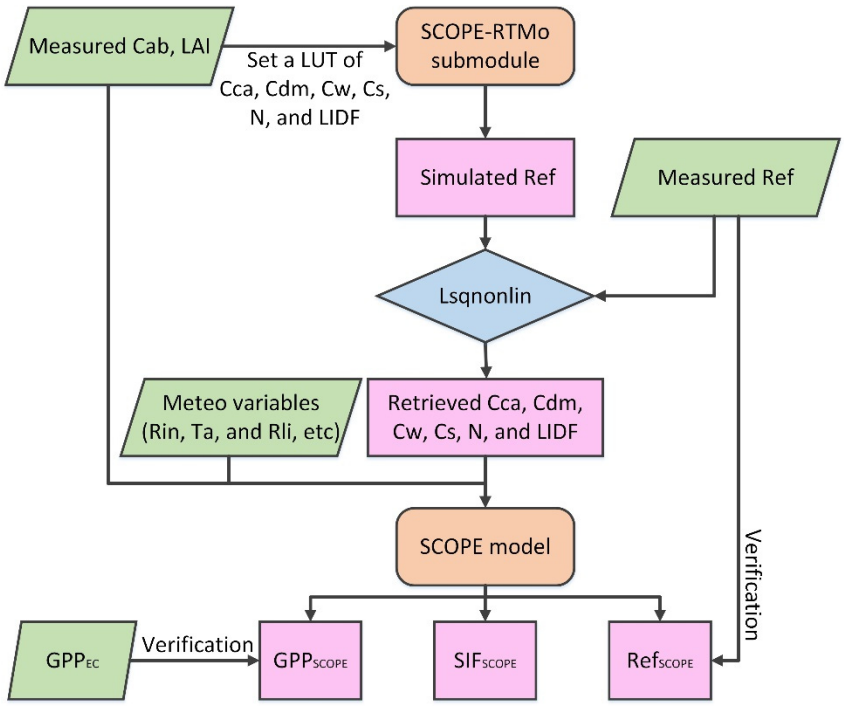

Figure 2. Flow chart of the inversion and simulation procedure using SCOPE model.

2.4. Evaluation of the Two SIF Estimation Approaches by Comparing with SCOPE Model

2.4.1. SIF Estimation of the CCC Approach

It was found that CCC (canopy chlorophyll concentration) had a non-linear logarithmic relationship with canopy SIF for the deciduous mixed forest plantation, which was used to estimate spatial SIF [25]. Thus, we supposed that the CCC might be an approach to estimate the diurnal dynamics of SIF. In the CCC approach, SIF is described as a logarithmic function of CCC as follows:

$$SIF_{CCC} = a \times In(CCC) + b \quad (2)$$

where CCC was calculated by the product of Cab and LAI.

2.4.2. SIF Estimation of the Backward Approach

The backward approach is a reverse process of GPP estimation. With the given leaf-based parameter, namely, $\frac{P_{apparent}}{c \times F_s}$, GPP was forward estimated using SIF measurements [26]. Therefore, we could reversely estimate SIF using GPP measurements and the parameter:

$$SIF_{BACK} = GPP_{EC} \times \frac{c \times F_s}{P_{apparent}} \quad (3)$$

where c is the correction coefficient, which is proven to be a typical constant of 0.0001 (mW m^{-2} sr^{-1} nm^{-1} per F_s count) [26].

However, the coefficient c was obtained under a given incident PAR at the light intensity of 600 µmol m^{-2} s^{-1} [26], so we improved the backward approach through a correction factor (k), a ratio of PAR_{leaf} and the given PAR.

$$SIF_{BACK*} = GPP_{EC} \times \frac{k \times c \times F_s}{P_{apparent}} \quad (4)$$

2.4.3. Evaluation Process of the Two Approaches

Taking SIF simulated by the SCOPE model (SIF_{SCOPE}) at the canopy level as a benchmark, we compared the diurnal variations in SIF estimated by both CCC and backward approaches with the SIF_{SCOPE} (Figure 3). The performances of relationships between SIF_{SCOPE} and SIF estimated from different approaches were evaluated by the coefficient of determination (R^2). Cab, F_s and $P_{apparent}$ were measured hourly; thereby, half-hourly GPP_{EC} and SIF_{SCOPE} were averaged to every hour to match the time resolution of the others. Due to a malfunction of the LI-6400XT, the erroneous observation data on 22 May was eliminated.

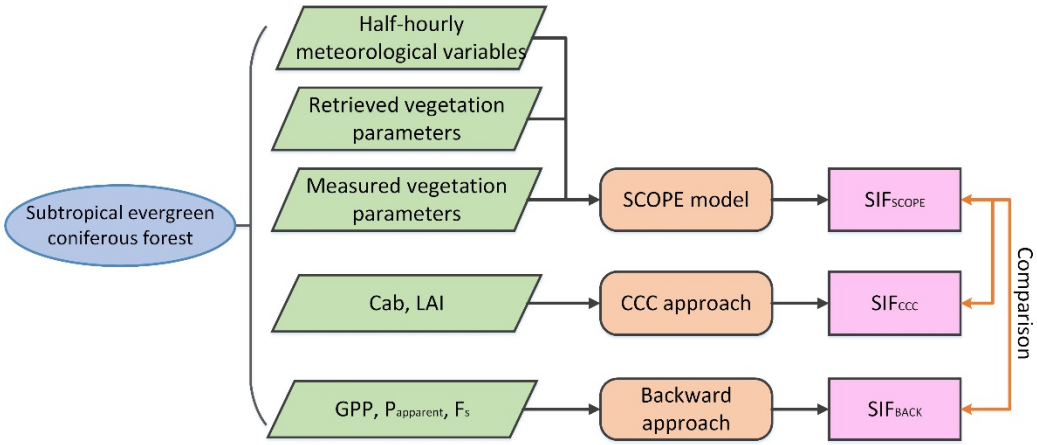

Figure 3. Schematic overview of SIF simulations and approach comparative analysis.

3. Results

3.1. Parameters Retrieved from In Situ Measurements for SCOPE Model

The leaf traits and canopy structure parameters, including Cab, Cca, Cs, Cw, Cdm, N, LIDFa, LIDFb and LAI, together govern the changes in the canopy reflectance. Based on the inversion procedure as shown in Figure 2, vegetation parameters including Cca, Cdm, Cw, Cs, N, LIDFa and LIDFb were retrieved on the eight fieldwork days (Table 3). Cab and LAI were obtained from field measurements. The results showed that the Cca varied from 2.86 μg cm^{-2} to 13.14 μg cm^{-2} on different days of the growing season, although Cab of the subtropical evergreen forest did not change significantly during the year (Table 1). Cdm and Cw remained almost stable at 0.02 and 0.05, respectively, during the whole growing season. N was also stable at 3, except for a relatively low value in July. Cs varied greatly throughout the year, showing higher values in spring and autumn and lower values in summer. The seasonal variation in LAI ranged from 4.85 m^2 m^{-2} to 4.24 m^2 m^{-2}, with the highest in July and lowest in November (Table 1). The seasonal variation in the pattern of LIDFa and LIDFb showed that the leaf inclination and its distribution both changed during the growing season. The model reproduced the measured canopy reflectance well with sum squared residuals (SSR) between 0.02 and 1.02 (Table 3). The results also showed that the simulated half-hourly GPP_{SCOPE} significantly correlated to the measured GPP_{EC} (R^2 = 0.80, $p < 0.001$, Figure 4). The linear relationship between GPP_{SCOPE} and GPP_{EC} was close to the 1:1 line, in spite of some data spread caused by the uncertainty of measured meteorological data and the simplify of the model processes. All these results proved that the SCOPE model could accurately retrieve the characteristics of leaf trait and canopy structure using the measured reflectance as a constraint.

Table 3. Retrieved parameters from measured canopy reflectance by SCOPE model on fieldwork days in 2017 for the subtropical evergreen coniferous forest at QYZ site.

Date	21 April	22 May	1 July	22 July	31 August	24 September	23 October	25 November
Cca	5.02	6.23	8.59	10.13	9.65	13.14	7.20	2.86
Cdm	0.02	0.02	0.02	0.02	0.02	0.02	0.02	0.02
Cw	0.050	0.05	0.049	0.050	0.050	0.049	0.050	0.050
Cs	0.72	0.34	0.64	0.25	0.26	0.24	0.33	0.69
N	3.00	3.00	3.00	2.17	3.00	2.96	3.00	3.00
LIDFa	0.91	−0.45	−0.51	−0.75	−0.89	−1.00	−0.97	0.00
LIDFb	−0.40	1.00	0.78	−0.09	1.00	0.65	1.00	1.00
SSR of Ref	1.02	0.16	0.14	0.02	0.04	0.02	0.04	0.28

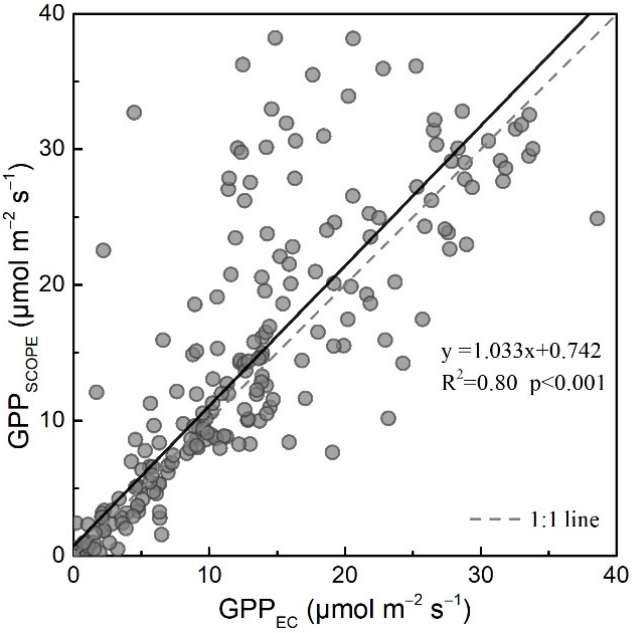

Figure 4. Comparison between measured GPP by eddy covariance system (GPP_{EC}) and simulated GPP by SCOPE model with retrieved vegetation parameters (GPP_{SCOPE}).

3.2. Diurnal Variations of Chlorophyll Fluorescence on Different Days during the Season

The canopy SIF simulated by the SCOPE model showed that canopy SIF_{687} and SIF_{760} had similar seasonal and diurnal variations (Figure 5a,b). They both reached their peaks in the summer across all these days and their daily maximum appeared near noon (12:00). The variations of canopy SIF closely correlated to the PAR incident above the canopy (SIF_{687}: $R^2 = 0.67$, $p < 0.001$; SIF_{760}: $R^2 = 0.89$, $p < 0.001$). Noticing that an extremely high PAR occurred on July 22th at both SIF_{687} and SIF_{760}. However, the GPP on that day did not show significant high values. We inferred that the excess light was emitted in the form of fluorescence to avert damage to the photosynthetic apparatus of the leaves. For the leaf level, the results illustrated that the value of F_s remained stable throughout one given daylight, although it held seasonal variations with lower in spring and higher in autumn. The variations in leaf PAR and photosynthesis rate (PAR_{leaf} and $P_{apparent}$) were consistent with these of PAR and GPP in the canopy (Figures 5 and 6). The $P_{apparent}$ also happened to be at the lowest level on 22 July with the high incident PAR (Figure 6c).

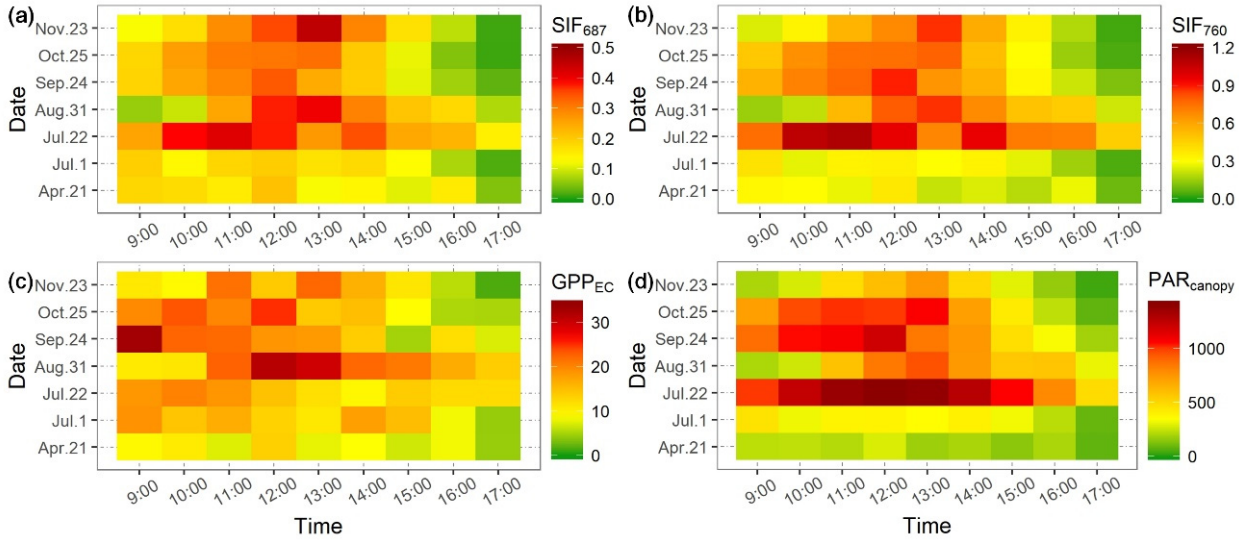

Figure 5. Diurnal variations of (**a**) canopy SIF at 687 nm (SIF_{687}), (**b**) canopy SIF at 760 nm (SIF_{760}), (**c**) canopy gross photosynthesis rate (GPP_{EC}) and (**d**) photosynthetic active radiance incident above the canopy (PAR_{canopy}) on fieldwork days in 2017.

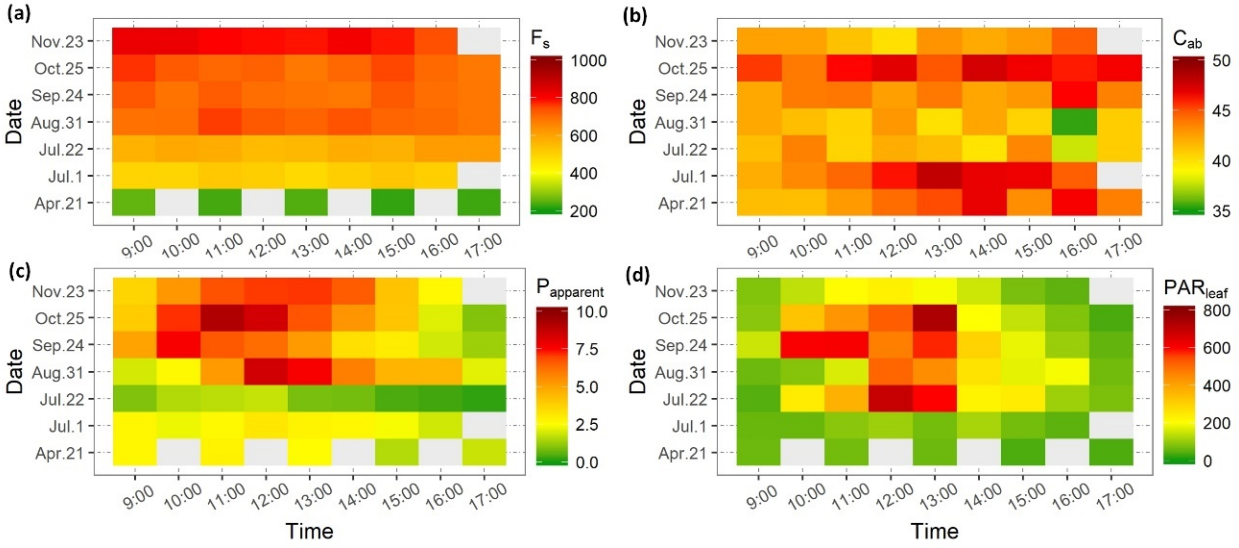

Figure 6. Diurnal variations of (**a**) leaf chlorophyll fluorescence (F_s), (**b**) leaf chlorophyll content (Cab), (**c**) leaf photosynthesis rate ($P_{apparent}$) and (**d**) photosynthetic active radiance incident on the leaves (PAR_{leaf}) on fieldwork days in 2017.

3.3. Evaluation of the CCC Approach Compared with the SCOPE Model

Figure 7 showed the logarithmic relationship between both SIF_{687} and SIF_{760} with the canopy chlorophyll concentration (CCC). The results showed that CCC ranged from 1.6 to 2.2 g m^{-2} during the experimental days and it could not capture the diurnal variation in either SIF_{687} or SIF_{760} (R^2 = 0.01 and R^2 = 0.00, respectively) with the logarithmic function. The CCC was the product of Cab and LAI. LAI remained unchanged throughout the day; thus, the diurnal variations of CCC depended on the Cab dynamics. However, the diurnal cycle of Cab is no obvious (Figure 6b). Thus, it can be seen that the CCC approach may not be suitable to track the diurnal variations in canopy SIF for the subtropical evergreen coniferous forest.

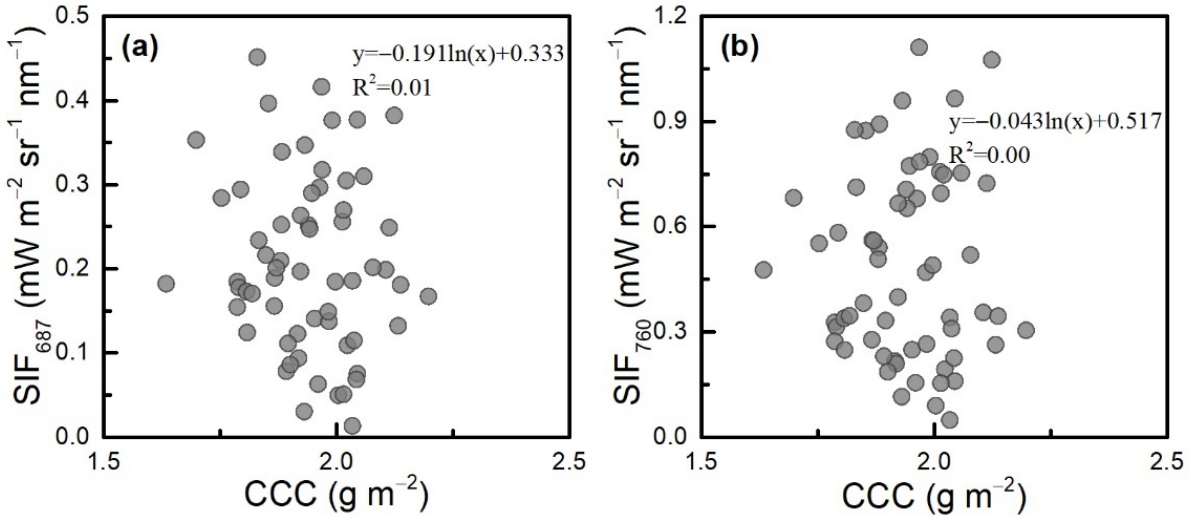

Figure 7. Logarithmic relationship between canopy chlorophyll concentration (CCC) and canopy SIF simulated by the SCOPE model (SIF_{SCOPE}). (**a**) CCC and SIF_{687}; (**b**) CCC and SIF_{760}.

3.4. Evaluation of the Backward Approach Compared with the SCOPE Model

Although the forward estimation of GPP by SIF observations was also designed for its temporal variation through seasons, we assessed the backward approach from GPP for the estimation of diurnal SIF dynamics. Figure 8 illustrated that the SIF_{BACK} using the direct backward approach did not significantly correlate with SIF_{687} (R^2 = 0.00) or SIF_{760} (R^2 = 0.03). It was also found that the high value of SIF_{BACK} was usually accompanied by high VPD. Considering the coefficient *c* in the raw forward approach was obtained under the given PAR, the correction factor *k* was used in our study to improve the approach. Using the improved backward approach, the SIF_{BACK*} accounted for 21% and 36% of temporal variations of SIF_{687} and SIF_{760}, respectively (R^2 = 0.21, $p < 0.001$; R^2 = 0.36, $p < 0.001$) (Figure 9a,b). The parabola regressions showed higher coefficients of determination (Figure 9), which was caused by the interference of high VPD on their positive correlation. After removing the abnormal points under drought stress (VPD > 2.7), the R^2 between SIF_{BACK*} and SIF_{SCOPE} improved to 0.53 for SIF_{687} ($p < 0.001$) and 0.72 for SIF_{760} ($p < 0.001$). The high VPD appeared on 22 July, when the subtropical forest experienced the seasonal drought. That also explained the lower GPP on this day. Thereby, the improved backward approach offers a new insight to estimate the diurnal canopy SIF dynamics without the water stress for subtropical coniferous forests.

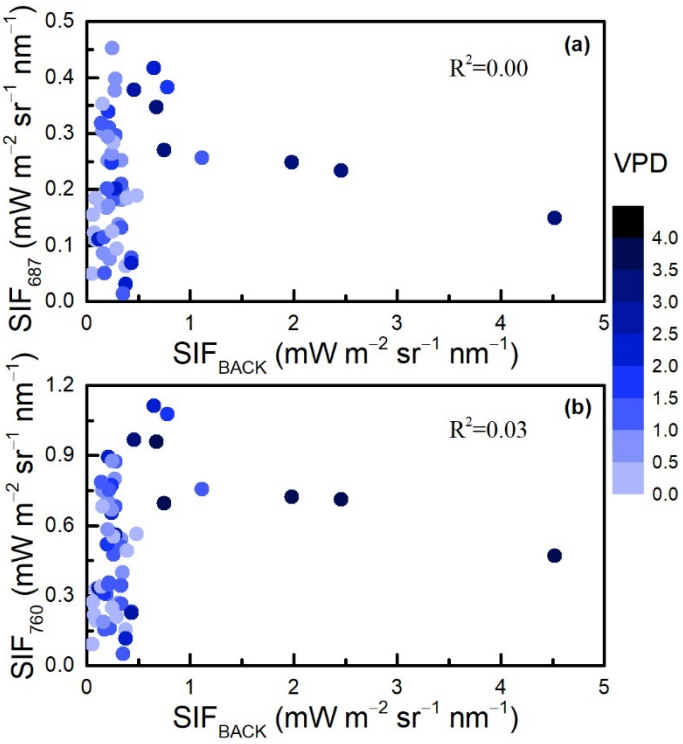

Figure 8. Comparison between canopy SIF estimated by the backward approach (SIF_{BACK}) and SIF_{SCOPE}. (**a**) SIF_{BACK} and SIF_{687}; (**b**) SIF_{BACK} and SIF_{760}.

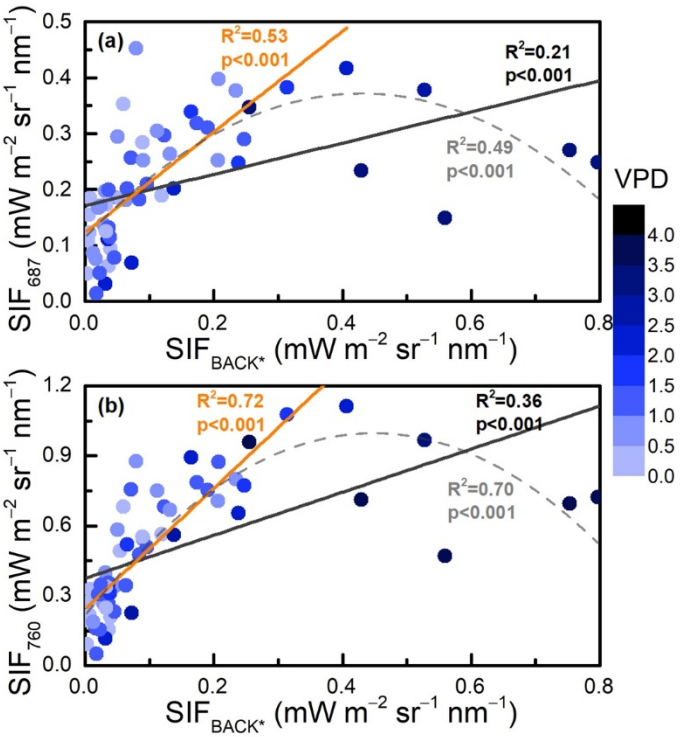

Figure 9. Comparison between canopy SIF estimated by the improved backward approach (SIF_{BACK*}) and SIF_{SCOPE} in all conditions (black line) or without drought (red line). (**a**) SIF_{BACK*} and SIF_{687}; (**b**) SIF_{BACK*} and SIF_{760}.

4. Discussion

4.1. Variations of Chlorophyll Fluorescence across Scales

In our study, the diurnal changes of the canopy SIF_{687} and SIF_{760} both showed typical single-peaks (Figure 5a,b), similar with the pattern of the irradiance incident above the canopy (Figure 5d).The variation in canopy SIF was dominated by the incident PAR above the canopy [42,43] and even more correlated to the absorbed PAR than GPP at short-time resolution [44]. In contrast, the variation of leaf F_s was non-obvious during the daytime (Figure 6a). Although the changes of leaf F_s are also related to the irradiance [45,46], the correlation was weakened in this study because of the average of F_s across leaves under different illumination due to the canopy geometry and varied solar irradiance. The incident irradiance field is required to be carefully characterized when we compare spectra-based SIF observations with PAM fluorescence measurements. The values and diurnal variations of PAR_{leaf} were both less than that of PAR_{canopy} in our results (Figures 5d and 6d). Another explanation might be the influence of different fluorescence emission bands for canopy SIF and F_s. SIF was usually measured at narrow wavelengths of O_2-A (687 nm) and O_2-B (760 nm) at canopy and landscape levels, whereas leaf F_s was measured over a broad spectral range between 700 and 715 nm. ChlF signal emitted from plants contains two crests in the range of 650–800 nm: One in the red spectral region (650–700 nm) with a maximum around 687 nm is mainly contributed by photosystem II (PSII) and the other in the near-infrared spectral region (700–800 nm) with a maximum near 740 nm is contributed by both photosystem I (PSI) and PSII [2]. Some model-based studies found the different sensitivities of SIF bands to leaf biochemistry and canopy structure [22,47].

Canopy SIF signal changed throughout the season. Canopy structure and leaf pigments matter on the variation of canopy SIF on the seasonal scale except for the illumination effect. Despite no sizeable seasonal variation of LAI, it displayed a slight increase in summer, which might lead to a rise in SIF emitted by total leaves. Leaf chlorophyll content modulates light absorption and fluorescence reabsorption, thereby regulating ChlF. Leaf chlorophyll content usually varies within the seasonal range, which is especially obvious due to leaf development and senescence [48,49]. However, the adjustments in chlorophyll content rarely occurred in these subtropical evergreen needles during the seasons. However, the retrieved carotenoid content varied a large range from 2.86 to 13.14 $\mu g\ cm^{-2}$. In addition, the effects of xanthophyll pigment also need to be taken into consideration to comprehend the seasonal variability of SIF for evergreen forests [5].

4.2. Explanations and Limitations of the CCC Approach and the Backward Approach

A non-linear logarithmic relationship ($R^2 > 0.9$, $p < 0.05$) was shown between simulated SIF by SCOPE model and CCC calculated by measured LAI and leaf Cab in a deciduous mixed forest plantation [25]. Based on this, the CCC approach was presented to estimate spatial SIF using the empirical relationship. However, the CCC did not capture the variations of SIF with the logarithmic function in our study (Figure 7). We infer that the different result is caused by the much fewer changes in the canopy chlorophyll that occurs in the evergreen forest than that in deciduous forest. In contrast to crops and deciduous plants, the canopy structure of forests is generally considered to be constant throughout the day. The LAI of the subtropical evergreen forests, which this study focused on, rarely even had large seasonal changes (Table 1). Therefore, the diurnal changes of SIF for the same canopy would hardly be disturbed by the canopy structure. The diurnal SIF dynamics estimated from the canopy chlorophyll concentration (CCC) mainly depended on the diurnal changes of leaf chlorophyll content. However, changes in the leaf chlorophyll content have rarely been found during the season (Table 1) nor the days (Figure 6b). There is a link between the amount of chlorophyll in leaves and the fluorescence emitted by chlorophyll, but the CCC typically represents a kind of potential fluorescence emission when all available chlorophyll is used at maximum efficiency. In fact, many regulation mechanisms make the efficiency could not fully used. The fewer canopy chlorophyll changes in the evergreen forest might be regulated by long-term environmental adaptation in the subtropical area. Radiance,

rather than canopy chlorophyll, matters for the fluorescence emission for evergreen forests. CCC could be a valuable approach to estimate spatial SIF at landscape scale using the empirical logarithmic relationship between CCC and SIF [25]. Still, the application of the CCC approach needs more evidence for the temporal SIF estimation, especially in the evergreen forests.

The backward approach estimates canopy SIF through an inverse way from [26], in which the estimation of GPP from the forward model using tower-based SIF and leaf-level F_s measurements agreed well with flux tower observations of GPP ($R^2 = 0.68$, $p < 0.0001$). We proved that the backward approach improved with the correction factor k could capture the diurnal dynamics of canopy SIF under normal weather conditions. Although the coefficient of determination of SIF_{BACK*} and SIF_{760} was higher than that of SIF_{BACK*} and SIF_{687}, but the values of SIF_{BACK*} and SIF_{687} were much closer. This might be caused by the different scattering and reabsorption effects on different wavelengths. One assumption of the backward approach is that both photosynthesis and fluorescence can be calculated as a product of the absorbed radiance and light conversion efficiency across different spatial levels. However, the top-of-canopy SIF observed from the tower is not merely the accumulative signal of SIF emitted by all leaves of the forest canopy but contains an additional term quantifying the effect of canopy scattering and reabsorption. Considering the escape probability of all SIF photons emitted from all leaves to the outer canopy (f_{esc}), we have SIF = APAR $\times$ ε_{FC} $\times$ f_{esc} [4,50,51]. In addition, the f_{esc} differed with the wavelength [52], which caused different degrees of underestimation of SIF_{687} and SIF_{760} using the backward approach (Figure 9). The f_{esc} and another correction factor FCVI, both designed to eliminate the effects of PAR scattering and reabsorption in the canopy, are used to downscale SIF from canopy level to leaf level, which is more directly related to photosynthesis [51–53]. The neglect of the scattering and reabsorption led to some uncertainties of the backward approach. Thus, we suggest the downscaling of canopy SIF signals with the f_{esc} or FCVI might benefit the application of the approach we proposed here if further research was made to improve the approach.

4.3. Impact of Seasonal Drought on the SIF Estimation

Despite the plentiful water and heat resources of the subtropical forests, changes in their seasonal cycles lead to frequent occurrences of seasonal drought, which affect the function of forest ecosystems (e.g., photosynthesis) [54,55]. In our study, the high VPD interfere the performance of the GPP backward approach for the SIF estimation. Photosynthesis contains light reaction and dark reaction, but these two reactions show different sensitivities to environmental factors such as illumination, temperature and water availability [56,57]. The emission of ChlF occurs in the light reaction stage, while the CO_2 fixation in the dark reaction stage is directly restricted by stomatal conductance. Water stress usually leads to the closure of stomata, thereby slowing the dark reaction rate and, thus, photosynthesis rate. The light and dark reactions are interdependent and restrict each other, so the decrease in stomatal conductance will theoretically-inevitably lead to the reduction of fluorescence quantum yield [58]. Some researchers found that the ChlF would decrease due to water stress while the vegetation canopy greenness would remain unchanged during drought [58,59]. Thereby, SIF anomaly was applied to monitor the drought events [60–62].

However, recent research found that with the treatment of stomatal closure, no obvious change occurred in SIF or F_s, despite evident reductions in stomatal conductance and carbon assimilation in leaves [63]. Responses of fluorescence emission and photosynthesis could decouple during drought, representing that vegetation photosynthesis might still be suppressed in spite of the variation in ChlF signal. Most works on SIF assumed a constant ratio of photosynthetic quantum efficiency (ε_P) and fluorescence quantum efficiency (ε_F) to establish the linear relationship between GPP and SIF, which was consistent with observations at large scales. Nevertheless, the assumption was questioned by a recent research, which suggested that SIF captured the variations of linear electron transport rate,

thus only providing insights into the light reactions of photosynthesis, without the dark reactions [17]. This explained why the SIF estimated by the backward approach under high VPD was poorly correlated with the SIF simulated by the SCOPE model. When fluorescence and photosynthesis are decoupled under environmental stress, the improved backward approach cannot be used validly. While the backward approach from GPP offers new insight into estimating canopy SIF, we suggest that the application of the approach under drought stress should be utilized properly and further experiments and research need to be done to interpret the influence of drought interfered with the stomata in response to future climate change.

5. Conclusions

In this study, we explored the practical approaches for the estimation of diurnal SIF dynamics using measured and simulated data for a typical subtropical evergreen coniferous forest site in eastern China. We described the diurnal changes in leaf and canopy chlorophyll fluorescence and compared the CCC (canopy chlorophyll concentration) approach and the backward GPP approach with the SCOPE model to evaluate their performance for estimating the temporal changes in canopy SIF. We found that the canopy SIF had similar seasonal and diurnal variations with the incident PAR above the canopy, while the leaf F_s remained stable throughout the daylight. The diurnal cycles of CCC relied on the leaf chlorophyll content, whose changes could not capture the canopy SIF dynamics. The raw backward approach did not work either. However, after improving the backward approach with a correction factor of normalized PAR_{leaf}, the simulated canopy SIF_{BACK^*} accounted for more than half of the diurnal variations of canopy SIF for the subtropical evergreen coniferous forest without water stress. This approach offers a unique insight into the estimation of diurnal canopy SIF and can help understand the response of vegetation to future climate change. In addition, the application of the approach should be utilized with care, especially under environmental stress.

Author Contributions: Conceptualization, S.W. and J.C.; methodology, J.C., B.C., M.A., L.M. and K.Z.; validation, J.C., B.C. and Y.L. (Yue Li); investigation, J.C., Y.L. (Yue Li), F.Y., X.W., Y.L. (Yuanyuan Liu), P.W., J.W., M.H. and Z.W.; writing—original draft preparation, J.C.; writing—review and editing, J.C., B.C. and M.A.; supervision, S.W.; funding acquisition, S.W. All authors have read and agreed to the published version of the manuscript.

Funding: This research was funded by the National Key Research and Development Program of China, grant number 2017YFC0503803; and the National Natural Science Foundation of China, grant number 41871342.

Data Availability Statement: The datasets analyzed in this study are managed by the Institute of Geographic Sciences and Natural Resources Research and are available upon request from the corresponding author.

Acknowledgments: The authors are grateful to the State Key Laboratory of Resources and Environmental Information System for the use of their facilities. We thank the staff of Qianyanzhou Ecological Research Station for their assistance in field measurements.

Conflicts of Interest: The authors declare no conflict of interest.

References

1. Maxwell, K.; Johnson, G.N. Chlorophyll fluorescence—A practical guide. *J. Exp. Bot.* **2000**, *51*, 659–668. [CrossRef]
2. Porcar-Castell, A.; Tyystjärvi, E.; Atherton, J.; Van der Tol, C.; Flexas, J.; Pfündel, E.E.; Moreno, J.; Frankenberg, C.; Berry, J.A. Linking chlorophyll a fluorescence to photosynthesis for remote sensing applications: Mechanisms and challenges. *J. Exp. Bot.* **2014**, *65*, 4065–4095. [CrossRef] [PubMed]
3. Guanter, L.; Frankenberg, C.; Dudhia, A.; Lewis, P.E.; Gómez-Dans, J.; Kuze, A.; Suto, H.; Grainger, R.G. Retrieval and global assessment of terrestrial chlorophyll fluorescence from GOSAT space measurements. *Remote Sens. Environ.* **2012**, *121*, 236–251. [CrossRef]

4. Guanter, L.; Zhang, Y.; Jung, M.; Joiner, J.; Voigt, M.; Berry, J.A.; Frankenberg, C.; Huete, A.R.; Zarco-Tejada, P.; Lee, J.-E. Global and time-resolved monitoring of crop photosynthesis with chlorophyll fluorescence. *Proc. Natl. Acad. Sci. USA* **2014**, *111*, E1327–E1333. [CrossRef] [PubMed]
5. Magney, T.S.; Bowling, D.R.; Logan, B.A.; Grossmann, K.; Stutz, J.; Blanken, P.D.; Burns, S.P.; Cheng, R.; Garcia, M.A.; Köhler, P. Mechanistic evidence for tracking the seasonality of photosynthesis with solar-induced fluorescence. *Proc. Natl. Acad. Sci. USA* **2019**, *116*, 11640–11645. [CrossRef] [PubMed]
6. Yang, X.; Tang, J.; Mustard, J.F.; Lee, J.E.; Rossini, M.; Joiner, J.; Munger, J.W.; Kornfeld, A.; Richardson, A.D. Solar-induced chlorophyll fluorescence that correlates with canopy photosynthesis on diurnal and seasonal scales in a temperate deciduous forest. *Geophys. Res. Lett.* **2015**, *42*, 2977–2987. [CrossRef]
7. Joiner, J.; Yoshida, Y.; Vasilkov, A.; Middleton, E. First observations of global and seasonal terrestrial chlorophyll fluorescence from space. *Biogeosciences* **2011**, *8*, 637–651. [CrossRef]
8. Joiner, J.; Guanter, L.; Lindstrot, R.; Voigt, M.; Vasilkov, A.; Middleton, E.; Huemmrich, K.; Yoshida, Y.; Frankenberg, C. Global monitoring of terrestrial chlorophyll fluorescence from moderate spectral resolution near-infrared satellite measurements: Methodology, simulations, and application to GOME-2. *Atmos. Meas. Tech.* **2013**, *6*, 2803–2823. [CrossRef]
9. Köhler, P.; Guanter, L.; Joiner, J. A linear method for the retrieval of sun-induced chlorophyll fluorescence from GOME-2 and SCIAMACHY data. *Atmos. Meas. Tech.* **2015**, *8*, 2589–2608. [CrossRef]
10. Frankenberg, C.; O'Dell, C.; Berry, J.; Guanter, L.; Joiner, J.; Köhler, P.; Pollock, R.; Taylor, T.E. Prospects for chlorophyll fluorescence remote sensing from the Orbiting Carbon Observatory-2. *Remote Sens. Environ.* **2014**, *147*, 1–12. [CrossRef]
11. Köhler, P.; Frankenberg, C.; Magney, T.S.; Guanter, L.; Joiner, J.; Landgraf, J. Global retrievals of solar-induced chlorophyll fluorescence with TROPOMI: First results and intersensor comparison to OCO-2. *Geophys. Res. Lett.* **2018**, *45*, 456–410, 463. [CrossRef] [PubMed]
12. Du, S.; Liu, L.; Liu, X.; Zhang, X.; Zhang, X.; Bi, Y.; Zhang, L. Retrieval of global terrestrial solar-induced chlorophyll fluorescence from TanSat satellite. *Sci. Bull.* **2018**, *63*, 1502–1512. [CrossRef]
13. Yang, X.; Shi, H.; Stovall, A.; Guan, K.; Miao, G.; Zhang, Y.; Zhang, Y.; Xiao, X.; Ryu, Y.; Lee, J.-E. FluoSpec 2—an automated field spectroscopy system to monitor canopy solar-induced fluorescence. *Sensors* **2018**, *18*, 2063. [CrossRef] [PubMed]
14. Zhou, X.; Liu, Z.; Xu, S.; Zhang, W.; Wu, J. An automated comparative observation system for sun-induced chlorophyll fluorescence of vegetation canopies. *Sensors* **2016**, *16*, 775. [CrossRef]
15. Julitta, T.; Burkart, A.; Colombo, R.; Rossini, M.; Schickling, A.; Migliavacca, M.; Cogliati, S.; Wutzler, T.; Rascher, U. Accurate measurements of fluorescence in the O2A and O2B band using the FloX spectroscopy system—Results and prospects. In Proceedings of the Potsdam GHG Flux Workshop: From Photosystems to Ecosystems, Potsdam, Germany, 26 October 2017; pp. 24–26.
16. Grossmann, K.; Frankenberg, C.; Magney, T.S.; Hurlock, S.C.; Seibt, U.; Stutz, J. PhotoSpec: A new instrument to measure spatially distributed red and far-red Solar-Induced Chlorophyll Fluorescence. *Remote Sens. Environ.* **2018**, *216*, 311–327. [CrossRef]
17. Gu, L.; Han, J.; Wood, J.D.; Chang, C.Y.Y.; Sun, Y. Sun-induced Chl fluorescence and its importance for biophysical modeling of photosynthesis based on light reactions. *New Phytol.* **2019**, *223*, 1179–1191. [CrossRef] [PubMed]
18. Du, S.; Liu, L.; Liu, X.; Guo, J.; Hu, J.; Wang, S.; Zhang, Y. SIFSpec: Measuring solar-induced chlorophyll fluorescence observations for remote sensing of photosynthesis. *Sensors* **2019**, *19*, 3009. [CrossRef]
19. Zhang, Y.; Zhang, Q.; Liu, L.; Zhang, Y.; Wang, S.; Ju, W.; Zhou, G.; Zhou, L.; Tang, J.; Zhu, X. ChinaSpec: A Network for Long-Term Ground-Based Measurements of Solar-Induced Fluorescence in China. *J. Geophys. Res. Biogeosci.* **2021**, *126*, e2020JG006042. [CrossRef]
20. Van der Tol, C.; Verhoef, W.; Timmermans, J.; Verhoef, A.; Su, Z. An integrated model of soil-canopy spectral radiances, photosynthesis, fluorescence, temperature and energy balance. *Biogeosciences* **2009**, *6*, 3109–3129. [CrossRef]
21. Hu, J.; Liu, X.; Liu, L.; Guan, L. Evaluating the performance of the SCOPE model in simulating canopy solar-induced chlorophyll fluorescence. *Remote Sens.* **2018**, *10*, 250. [CrossRef]
22. Zhang, Y.; Guanter, L.; Berry, J.A.; van der Tol, C.; Yang, X.; Tang, J.; Zhang, F. Model-based analysis of the relationship between sun-induced chlorophyll fluorescence and gross primary production for remote sensing applications. *Remote Sens. Environ.* **2016**, *187*, 145–155. [CrossRef]
23. Malenovský, Z.; Regaieg, O.; Yin, T.; Lauret, N.; Guilleux, J.; Chavanon, E.; Duran, N.; Janoutová, R.; Delavois, A.; Meynier, J. Discrete anisotropic radiative transfer modelling of solar-induced chlorophyll fluorescence: Structural impacts in geometrically explicit vegetation canopies. *Remote Sens. Environ.* **2021**, *263*, 112564. [CrossRef]
24. Verrelst, J.; Rivera, J.P.; van der Tol, C.; Magnani, F.; Mohammed, G.; Moreno, J. Global sensitivity analysis of the SCOPE model: What drives simulated canopy-leaving sun-induced fluorescence? *Remote Sens. Environ.* **2015**, *166*, 8–21. [CrossRef]
25. Sinha, S.K.; Padalia, H.; Patel, N.; Chauhan, P. Estimation of Seasonal Sun-Induced Fluorescence Dynamics of Indian Tropical Deciduous Forests using SCOPE and Sentinel-2 MSI. *Int. J. Appl. Earth Obs. Geoinf.* **2020**, *91*, 102155. [CrossRef]
26. Yang, H.; Yang, X.; Zhang, Y.; Heskel, M.A.; Lu, X.; Munger, J.W.; Sun, S.; Tang, J. Chlorophyll fluorescence tracks seasonal variations of photosynthesis from leaf to canopy in a temperate forest. *Glob. Chang. Biol.* **2017**, *23*, 2874–2886. [CrossRef] [PubMed]
27. Yu, G.; Chen, Z.; Piao, S.; Peng, C.; Ciais, P.; Wang, Q.; Li, X.; Zhu, X. High carbon dioxide uptake by subtropical forest ecosystems in the East Asian monsoon region. *Proc. Natl. Acad. Sci. USA* **2014**, *111*, 4910–4915. [CrossRef]

28. Wang, J.; Feng, L.; Palmer, P.I.; Liu, Y.; Fang, S.; Bösch, H.; O'Dell, C.W.; Tang, X.; Yang, D.; Liu, L. Large Chinese land carbon sink estimated from atmospheric carbon dioxide data. *Nature* **2020**, *586*, 720–723. [CrossRef] [PubMed]
29. Wen, X.; Yu, G.; Sun, X.; Liu, Y. Turbulence flux measurement above the overstory of a subtropical Pinus plantation over the hilly region in southeastern China. *Sci. China Ser. D-Earth Sci.* **2005**, *48*, 63.
30. Zhang, Q.; Ju, W.; Chen, J.M.; Wang, H.; Yang, F.; Fan, W.; Huang, Q.; Zheng, T.; Feng, Y.; Zhou, Y. Ability of the photochemical reflectance index to track light use efficiency for a sub-tropical planted coniferous forest. *Remote Sens.* **2015**, *7*, 16938–16962. [CrossRef]
31. Reichstein, M.; Falge, E.; Baldocchi, D.; Papale, D.; Aubinet, M.; Berbigier, P.; Bernhofer, C.; Buchmann, N.; Gilmanov, T.; Granier, A. On the separation of net ecosystem exchange into assimilation and ecosystem respiration: Review and improved algorithm. *Glob. Chang. Biol.* **2005**, *11*, 1424–1439. [CrossRef]
32. Hilker, T.; Nesic, Z.; Coops, N.C.; Lessard, D. A new, automated, multiangular radiometer instrument for tower-based observations of canopy reflectance (AMSPEC II). *Instrum. Sci. Technol.* **2010**, *38*, 319–340. [CrossRef]
33. Wang, S.; Li, Y.; Ju, W.; Chen, B.; Chen, J.; Croft, H.; Mickler, R.A.; Yang, F. Estimation of leaf photosynthetic capacity from leaf chlorophyll content and leaf age in a subtropical evergreen coniferous plantation. *J. Geophys. Res. Biogeosci.* **2020**, *125*, e2019JG005020. [CrossRef]
34. Larcher, W.; Cernusca, A. Mikrocomputergesteuerte mobile Anlage zum fluorometrischen Nachweis von Photosynthesestörungen. *Ber. Der Oesterreichische Akadamie Wiss.* **1985**, *194*, 45–64.
35. Wohlfahrt, G.; Gu, L. The many meanings of gross photosynthesis and their implication for photosynthesis research from leaf to globe. *PlantCell Environ.* **2015**, *38*, 2500. [CrossRef] [PubMed]
36. Kobayashi, H.; Ryu, Y.; Baldocchi, D.D.; Welles, J.M.; Norman, J.M. On the correct estimation of gap fraction: How to remove scattered radiation in gap fraction measurements? *Agric. For. Meteorol.* **2013**, *174*, 170–183. [CrossRef]
37. Gower, S.T.; Kucharik, C.J.; Norman, J.M. Direct and indirect estimation of leaf area index, fAPAR, and net primary production of terrestrial ecosystems. *Remote Sens. Environ.* **1999**, *70*, 29–51. [CrossRef]
38. Zhu, G.; Ju, W.; Chen, J.M.; Gong, P.; Xing, B.; Zhu, J. Foliage clumping index over China's landmass retrieved from the MODIS BRDF parameters product. *IEEE Trans. Geosci. Remote Sens.* **2011**, *50*, 2122–2137. [CrossRef]
39. Yang, P.; Prikaziuk, E.; Verhoef, W.; van der Tol, C. SCOPE 2.0: A model to simulate vegetated land surface fluxes and satellite signals. *Geosci. Model Dev.* **2021**, *14*, 4697–4712. [CrossRef]
40. van der Tol, C.; Rossini, M.; Cogliati, S.; Verhoef, W.; Colombo, R.; Rascher, U.; Mohammed, G. A model and measurement comparison of diurnal cycles of sun-induced chlorophyll fluorescence of crops. *Remote Sens. Environ.* **2016**, *186*, 663–677. [CrossRef]
41. Yang, P.; van der Tol, C.; Verhoef, W.; Damm, A.; Schickling, A.; Kraska, T.; Muller, O.; Rascher, U. Using reflectance to explain vegetation biochemical and structural effects on sun-induced chlorophyll fluorescence. *Remote Sens. Environ.* **2019**, *231*, 110996. [CrossRef]
42. Chen, J.; Zhang, Q.; Chen, B.; Zhang, Y.; Ma, L.; Li, Z.; Zhang, X.; Wu, Y.; Wang, S.; A Mickler, R. Evaluating Multi-Angle Photochemical Reflectance Index and Solar-Induced Fluorescence for the Estimation of Gross Primary Production in Maize. *Remote Sens.* **2020**, *12*, 2812. [CrossRef]
43. Paul-Limoges, E.; Damm, A.; Hueni, A.; Liebisch, F.; Eugster, W.; Schaepman, M.E.; Buchmann, N. Effect of environmental conditions on sun-induced fluorescence in a mixed forest and a cropland. *Remote Sens. Environ.* **2018**, *219*, 310–323. [CrossRef]
44. Yang, K.; Ryu, Y.; Dechant, B.; Berry, J.A.; Hwang, Y.; Jiang, C.; Kang, M.; Kim, J.; Kimm, H.; Kornfeld, A. Sun-induced chlorophyll fluorescence is more strongly related to absorbed light than to photosynthesis at half-hourly resolution in a rice paddy. *Remote Sens. Environ.* **2018**, *216*, 658–673. [CrossRef]
45. Cerovic, Z.; Goulas, Y.; Gorbunov, M.; Briantais, J.-M.; Camenen, L.; Moya, I. Fluorosensing of water stress in plants: Diurnal changes of the mean lifetime and yield of chlorophyll fluorescence, measured simultaneously and at distance with a τ-LIDAR and a modified PAM-fluorimeter, in maize, sugar beet, and kalanchoë. *Remote Sens. Environ.* **1996**, *58*, 311–321. [CrossRef]
46. Flexas, J.; Briantais, J.-M.; Cerovic, Z.; Medrano, H.; Moya, I. Steady-state and maximum chlorophyll fluorescence responses to water stress in grapevine leaves: A new remote sensing system. *Remote Sens. Environ.* **2000**, *73*, 283–297. [CrossRef]
47. Verrelst, J.; van der Tol, C.; Magnani, F.; Sabater, N.; Rivera, J.P.; Mohammed, G.; Moreno, J. Evaluating the predictive power of sun-induced chlorophyll fluorescence to estimate net photosynthesis of vegetation canopies: A SCOPE modeling study. *Remote Sens. Environ.* **2016**, *176*, 139–151. [CrossRef]
48. García-Plazaola, J.I.; Becerril, J.M. Seasonal changes in photosynthetic pigments and antioxidants in beech (*Fagus sylvatica*) in a Mediterranean climate: Implications for tree decline diagnosis. *Funct. Plant Biol.* **2001**, *28*, 225–232. [CrossRef]
49. Lu, C.; Lu, Q.; Zhang, J.; Kuang, T. Characterization of photosynthetic pigment composition, photosystem II photochemistry and thermal energy dissipation during leaf senescence of wheat plants grown in the field. *J. Exp. Bot.* **2001**, *52*, 1805–1810. [CrossRef]
50. Dechant, B.; Ryu, Y.; Badgley, G.; Zeng, Y.; Berry, J.A.; Zhang, Y.; Goulas, Y.; Li, Z.; Zhang, Q.; Kang, M. Canopy structure explains the relationship between photosynthesis and sun-induced chlorophyll fluorescence in crops. *Remote Sens. Environ.* **2020**, *241*, 111733. [CrossRef]
51. Zeng, Y.; Badgley, G.; Dechant, B.; Ryu, Y.; Chen, M.; Berry, J.A. A practical approach for estimating the escape ratio of near-infrared solar-induced chlorophyll fluorescence. *Remote Sens. Environ.* **2019**, *232*, 111209. [CrossRef]

52. Liu, X.; Liu, L.; Hu, J.; Guo, J.; Du, S. Improving the potential of red SIF for estimating GPP by downscaling from the canopy level to the photosystem level. *Agric. For. Meteorol.* **2020**, *281*, 107846. [CrossRef]
53. Yang, P.; van der Tol, C.; Campbell, P.K.; Middleton, E.M. Fluorescence Correction Vegetation Index (FCVI): A physically based reflectance index to separate physiological and non-physiological information in far-red sun-induced chlorophyll fluorescence. *Remote Sens. Environ.* **2020**, *240*, 111676. [CrossRef]
54. Li, P.; Zhang, L.; Yu, G.; Liu, C.; Ren, X.; He, H.; Liu, M.; Wang, H.; Zhu, J.; Ge, R. Interactive effects of seasonal drought and nitrogen deposition on carbon fluxes in a subtropical evergreen coniferous forest in the East Asian monsoon region. *Agric. For. Meteorol.* **2018**, *263*, 90–99. [CrossRef]
55. Mi, N.; Yu, G.; Wen, W.; Sun, X.; Wang, S.; Zhang, L.; Song, X. Use of ecosystem flux data and a simulation model to examine seasonal drought effects on a subtropical coniferous forest. *Asia-Pac. J. Atmos. Sci.* **2009**, *45*, 207–220.
56. Ensminger, I.; Busch, F.; Huner, N.P. Photostasis and cold acclimation: Sensing low temperature through photosynthesis. *Physiol. Plant.* **2006**, *126*, 28–44. [CrossRef]
57. Huner, N.; Maxwell, D.; Gray, G.; Savitch, L.; Krol, M.; Ivanov, A.; Falk, S. Sensing environmental temperature change through imbalances between energy supply and energy consumption: Redox state of photosystem II. *Physiol. Plant.* **1996**, *98*, 358–364. [CrossRef]
58. Daumard, F.; Champagne, S.; Fournier, A.; Goulas, Y.; Ounis, A.; Hanocq, J.-F.; Moya, I. A field platform for continuous measurement of canopy fluorescence. *IEEE Trans. Geosci. Remote Sens.* **2010**, *48*, 3358–3368. [CrossRef]
59. Flexas, J.; Escalona, J.M.; Evain, S.; Gulías, J.; Moya, I.; Osmond, C.B.; Medrano, H. Steady-state chlorophyll fluorescence (Fs) measurements as a tool to follow variations of net CO2 assimilation and stomatal conductance during water-stress in C3 plants. *Physiol. Plant.* **2002**, *114*, 231–240. [CrossRef]
60. Sun, Y.; Fu, R.; Dickinson, R.; Joiner, J.; Frankenberg, C.; Gu, L.; Xia, Y.; Fernando, N. Drought onset mechanisms revealed by satellite solar-induced chlorophyll fluorescence: Insights from two contrasting extreme events. *J. Geophys. Res. Biogeosci.* **2015**, *120*, 2427–2440. [CrossRef]
61. Yang, J.; Tian, H.; Pan, S.; Chen, G.; Zhang, B.; Dangal, S. Amazon drought and forest response: Largely reduced forest photosynthesis but slightly increased canopy greenness during the extreme drought of 2015/2016. *Glob. Chang. Biol.* **2018**, *24*, 1919–1934. [CrossRef] [PubMed]
62. Yoshida, Y.; Joiner, J.; Tucker, C.; Berry, J.; Lee, J.-E.; Walker, G.; Reichle, R.; Koster, R.; Lyapustin, A.; Wang, Y. The 2010 Russian drought impact on satellite measurements of solar-induced chlorophyll fluorescence: Insights from modeling and comparisons with parameters derived from satellite reflectances. *Remote Sens. Environ.* **2015**, *166*, 163–177. [CrossRef]
63. Marrs, J.; Reblin, J.; Logan, B.; Allen, D.; Reinmann, A.; Bombard, D.; Tabachnik, D.; Hutyra, L. Solar-induced fluorescence does not track photosynthetic carbon assimilation following induced stomatal closure. *Geophys. Res. Lett.* **2020**, *47*, e2020GL087956. [CrossRef]